Available online at www.sciencedirect.com
ScienceDirect
Comput. Methods Appl. Mech. Engrg. 279 (2014) 536–553
Computer methods in applied mechanics and engineering
www.elsevier.com/locate/cma

Bayesian calibration of the constants of the k–ε turbulence model for a CFD model of street canyon flow

Serge Guillas[a], Nina Glover[b,*], Liora Malki-Epshtein[b]

[a] *Department of Statistical Science, UCL, London, UK*
[b] *Department of Civil, Environmental and Geomatic Engineering, UCL, London, UK*

Received 18 June 2012; received in revised form 28 March 2014; accepted 3 June 2014
Available online 27 June 2014

Abstract

In this paper we carry out a Bayesian calibration for uncertainty analysis in Computational Fluid Dynamics modelling of urban flows. Taking the case of airflow in a regular street canyon, and choosing turbulent kinetic energy (TKE) as our quantity of interest, we calibrate 3-D CFD simulations against wind tunnel observations. We focus our calibration on the model constants contained within the standard RANS k–ε turbulence model and the uncertainties relating to these values. Thus we are able to narrow down the space of k–ε model constants which provide the best match with experimental data and quantify the uncertainty relating to both the k–ε model constants in the case of street canyon flow and the TKE outputs of the CFD simulation. Furthermore, we are able to construct a statistical emulator of the CFD model. Finally, we provide predictions of TKE based on the emulator and the estimated bias between model and observations, accompanied with uncertainties in these predictions.

Keywords: Uncertainty quantification; Emulation; Computational fluid dynamics; Turbulence modelling; k–ε model

1. Introduction

The use of Computational Fluid Dynamics modelling in the built environment is widespread for indoor applications; however the successful and systematic application of CFD for the outdoor environment is still hindered by the prohibitive cost of field measurements and lack of validation of turbulent characteristics and boundary conditions for a variety of urban atmospheric boundary layer flows. The problem is exacerbated further by the geometric complexity of the built environment and the difficulties in modelling flow around arrays of building obstacles. An in-depth understanding of the airflow processes within street canyons is important to fully understand the pollutant dispersion within these spaces as well as issues relating to pedestrian comfort and energy use. CFD has had a larger role to play in modelling this process in recent years as computer power and quality of commercial software have increased. Built environment researchers and practitioners commonly use commercial CFD software for their simulations and employ

* Corresponding author.
E-mail address: n.glover@ucl.ac.uk (N. Glover).

http://dx.doi.org/10.1016/j.cma.2014.06.008

default settings following simple guidelines. Thus the k–ε model is a popular choice as it is simple and fast to run. However it has not been extensively validated for urban boundary layers and is not entirely suitable in regions of high streamline curvature. By understanding and quantifying some of the uncertainties relating to these CFD models of the outdoor environment, we can move towards improved modelling guidelines and better models for urban planners and street designers. Better models will ultimately help to assess and mitigate risk to human health from sources such as pollution and the release of toxic gases, in order to inform policy and decision making in the urban environment, which now houses over half of the global population.

Here we follow the full Bayesian calibration framework of Kennedy and O'Hagan [1], which involves representing bias and computer model outputs as Gaussian processes, to investigate how the sophisticated tuning of the empirical constants contained within the chosen turbulence model can improve the prediction of the turbulent quantities within a regular street canyon. Thus, we attempt a calibration of the constants contained in the Standard k–ε turbulence model for the particular case study of flow over a symmetrical, homogeneous street canyon at aspect ratio (height to width of the street) of $H/W = 1$ and a Reynolds number of 5×10^4. ANSYS CFX is used to create the CFD model, which is then calibrated against measurements of turbulent kinetic energy, TKE, obtained in wind tunnel laboratory experiments [2]. It was decided to calibrate against the TKE outputs due to the noted difficulties the k–ε model has at predicting TKE levels within street canyons. The accurate prediction of these values is particularly important for modelling pollution dispersion. Under low wind conditions the turbulence levels can have a large impact on how the pollutants are distributed throughout the street.

This calibration process allows us to:

(1) evaluate a small systematic bias of the CFD model;

(2) narrow down the set of parameter values that provides the best match between the CFD model outputs and the observations;

(3) construct a fast statistical surrogate (also called emulator) of the CFD model;

(4) use the emulator to quantify the uncertainty of the turbulent kinetic energy outputs resulting from both uncertainties in the CFD parameterization, the numerical code itself and measurement errors: this propagation of uncertainties would be an extremely computationally demanding task without emulation.

This paper starts with a discussion on uncertainty quantification and model verification for CFD models. Then we give a brief introduction to the standard k–ε model followed by a summary of its use for urban atmospheric boundary layer flow. A description of the experimental and CFD set up is then given, for this particular case study of a symmetrical street canyon, followed by an explanation of the Bayesian Calibration process. Finally, we discuss the results and the conclusions gained from them.

1.1. Uncertainty quantification in CFD

There are several sources of uncertainty present within CFD models. These can come from the model inputs, the form of the model, the assumptions made in the mathematical model, and numerical approximation errors which are due to the differential equations being approximated rather than solved explicitly (an example of this would be discretization error). Different techniques can be applied to tackle each type of uncertainty. Model verification deals with the uncertainties relating to numerical approximation. It is a way of providing evidence that the computer model accurately represents the conceptual model of the system. Model validation is used to ensure the computer model is an accurate representation of the physical system of interest and deals with the uncertainty related to model form. This involves comparing the CFD output against experimental data. A full description of these types of uncertainties and statistical methods for quantifying them can be found in Roy and Oberkampf [3].

Uncertainty quantification in CFD and in numerical models in general can be done using a variety of statistical methods. One such method, Polynomial Chaos, is discussed in detail in Najm [4] with examples of applications of this technique to different types of flows such as incompressible and reacting flows. Le Maitre et al. [5] applied this technique to incompressible flow in a micro channel with low Reynolds Number.

Although uncertainty quantification is an important topic within CFD particularly within the field of turbulence models, it is not routinely addressed in CFD-based studies. However there are a number of studies that have demonstrated different statistical techniques to address the issue of uncertainty within RANS turbulence models. One such study conducted by Dunn et al. [6] looked at the uncertainty contained within the model coefficients of the k–ε model. They used the Latin Hypercube Sampling method rather than Bayesian Calibration techniques to investigate

these uncertainties in the case of flow over a backward step and found that model coefficients had a significant effect on stream wise mean velocity, turbulence intensity, reattachment point location, pressure and wall shear stress.

An example of Bayesian Calibration of RANS turbulence models is given by Oliver and Moser [7]. The Bayesian approach was used to analyse both model and parameter uncertainty within several types of turbulence models and was then applied to the case of incompressible channel flow. Oliver and Moser [7] were able to make a comparison between different uncertainty quantification models as well as different turbulence models and found both to impact the quantity of interest (QoI's). They found that after calibration the Chien k–ε model gave a prediction of the QoI's with an uncertainty of approximately $\pm 4\%$. Another example of a study which used Bayesian Calibration to assess uncertainty within RANS models is Cheung et al. [8]. The Spalart–Allmaras turbulence model was used to model the case of an incompressible boundary layer flow. Seven constants within the SA model were calibrated against experimental data, and predictions of the quantities of interest were produced. In this work the plausibility of competing models for uncertainty evaluation was investigated. Edeling et al. [9] recently calibrated four constants in the Launder–Sharma k–ε model for 13 wall-bounded turbulent boundary layer flows at a variety of pressure gradients. They analysed uncertainties relating to the k–ε model constants and their propagation throughout the model to the QoI of velocity profiles. The 13 separate Bayesian calibrations were carried out on the boundary layer velocity profiles generated by a specialized 2-D, compressible boundary-layer approximation mode applied to flow over a curved aerofoil-shaped surface.

In our study the Standard k–ε turbulence model will be applied for the particular case study of flow over a symmetrical, homogeneous street canyon at aspect ratio (height to width of the street) of $H/W = 1$ and a Reynolds number of 5×10^4. We will be focusing on the uncertainties relating to the model inputs. In the scenario of an urban boundary layer flow, these are a large source of uncertainty, as the standard k–ε model has not been extensively validated for this complex case. Although these uncertainties are well acknowledged among the community of CFD practitioners, it is not a standard procedure to account for them in either the model set up or when presenting the output of the CFD model. Here we will look at how we can address such uncertainties and those relating to the k–ε model constants and how they can be propagated throughout the model to the quantities of interest (QoI's), which are mainly the TKE profiles within the street canyon. Cheung et al. [8], having made the first step in their calibration of a CFD model, highlighted for future research the areas of comparative uncertainty analysis of RANS turbulence models, as well as the use of statistical emulators to save computing time on computationally expensive CFD models. We construct here such an emulator of the RANS model.

1.2. Turbulence models

Turbulent flow is characterized by random fluctuations of velocity. It is possible to model turbulent flow within CFD without any adjustments to the Navier–Stokes equations. This type of simulation is known as direct numerical simulation (DNS) and is prohibitively computationally expensive. Turbulence models used within CFD simulations enable the capture of the main features of the flow without having to explicitly model all the details of the turbulence, thus saving on computer costs. Large eddy simulations (LES) save computing time compared with DNS by explicitly resolving only the large and most important turbulent eddies in the flow and approximating the smaller scale turbulence. However this technique is either still out of reach for simulation of the outdoor environment, or when computational power is available, is very difficult to tune, which may make it imprecise, see Blocken et al. [10] and references therein.

We can reduce the amount of computing power needed by focusing on the mean properties of the flow. This results in the Reynolds-Averaged Navier–Stokes (RANS) equations. These equations contain correlations of the fluctuating velocity components $\overline{u_i' u_j'}$ which are known as the Reynolds stresses. The turbulence model is a way of closing the RANS equations by approximating the Reynolds stress. The Standard k–ε turbulence model is a popular choice of RANS model.

1.3. The standard k–ε model

The formulation of this model is as follows:

The Reynolds stresses $\overline{u_i' u_j'}$ are related to the shear stress of the flow τ_{ij} by the following equation:

$$\tau_{ij} = -\rho \overline{u_i' u_j'} \tag{1}$$

Table 1
Standard values and ranges considered in the calibration used for model constants.

	C_μ	$C_{\varepsilon 1}$	$C_{\varepsilon 2}$	σ_ε	σ_k
Standard values	0.09	1.44	1.92	1.3	1.0
Ranges	0.01−0.15	1−1.5	1.1−2.5	See (9)	0.5−2.5

where ρ is the density of the fluid. We can find the value for τ, and hence $\overline{u_i' u_j'}$, from the following equation:

$$\tau_{ij} = \mu_t \left(\frac{\partial \bar{u}_i}{\partial x_j} + \frac{\partial \bar{u}_j}{\partial x_i} \right) - \frac{2}{3} \rho k \delta_{ij} \tag{2}$$

where μ_t is the turbulent viscosity. In the case of the standard k–ε turbulence model, turbulent viscosity is defined as

$$\mu_t = \rho C_\mu \frac{k^2}{\varepsilon} \tag{3}$$

where C_μ is a model constant [11].

By solving the following differential equations for the turbulent kinetic energy, k, and the turbulent dissipation, ε we can find a value for μ_t [11]:

$$\frac{D(\rho k)}{Dt} = \frac{\partial}{\partial x_j} \left(\left(\mu + \frac{\mu_t}{\sigma_k} \right) \frac{\partial k}{\partial x_j} \right) + \tau_{ij} \frac{\partial \bar{u}_i}{\partial x_j} - \rho \varepsilon \tag{4}$$

$$\frac{D(\rho \varepsilon)}{Dt} = \frac{\partial}{\partial x_j} \left(\left(\mu + \frac{\mu_t}{\sigma_\varepsilon} \right) \frac{\partial \varepsilon}{\partial x_j} \right) + C_{\varepsilon_1} \frac{\varepsilon}{k} \tau_{ij} \frac{\partial \bar{u}_i}{\partial x_j} - C_{\varepsilon 2} \rho \frac{\varepsilon^2}{k} \tag{5}$$

where σ_k, σ_ε, $C_{\varepsilon 1}$, $C_{\varepsilon 2}$ and C_μ are all empirical model constants. The default values for these constants in most commercial CFD softwares, including ANSYS CFX tested here, are shown in Table 1. These values follow the original formulation of Launder and Spalding [12], who obtained them through data fitting for a wide range of flows.

1.4. The use of the standard k–ε model for built environment applications

When using CFD to simulate flow within the built environment it is important to generate the correct boundary layer flow at the area of interest. A common problem of creating a neutral equilibrium atmospheric boundary layer is an acceleration in the velocity at ground level and a decay in turbulence profile as we move downstream. This occurs when the boundary conditions, the turbulence model and its associated constants are not consistent with each other [13], for example when the velocity, turbulent kinetic energy and turbulent dissipation profiles specified at the inlet do not satisfy the transportation equations of the Standard k–ε model. The most common method to deal with this is to derive the inlet profiles for turbulent kinetic energy, k, and turbulent dissipation rate, ε, directly from the k–ε model formulation. This was the approach of Richards and Hoxey [14] who recommended the following formulation for the inlet profiles, which is consistent with the Standard k–ε model:

1. Inlet Velocity Profile:

$$u = \frac{u_*}{\kappa} \ln \left(\frac{z + z_0}{z_0} \right) \tag{6}$$

where u_* is the frictional velocity, κ is the von Karman constant and z_0 is the aerodynamic roughness length.

2. Turbulent Kinetic Energy profile:

$$k = \frac{u_*^2}{\sqrt{C_\mu}}. \tag{7}$$

3. Turbulent Dissipation profile:

$$\varepsilon = \frac{u_*^3}{\kappa (z + z_0)}. \tag{8}$$

These profiles are commonly used when simulating flow over an urban region due to their ease of implementation and the fact that horizontal homogeneity can be achieved. However research has shown that comparisons of these profiles with either real life atmospheric boundary layer data or wind tunnel data showed an under-prediction of TKE, and also found TKE to be non-uniform with height, which is not reflected in the profiles. Ideally these inlet profiles would be changed to give a better match with the available data, however changing the values at the inlet for k and ε would result in an inconsistency between the boundary conditions, the k–ε turbulence model and its constants. As stated before this would lead to a decay in the profiles as we move downstream of the inlet. To overcome the issue of under-prediction of TKE at the inlet several authors have altered the value of C_μ. However as noted by Richards and Norris [13] altering the values of the Standard k–ε model constants should be done with care as the following relationship must still hold:

$$\sigma_\varepsilon = \frac{\kappa^2}{\sqrt{C_\mu}(C_{\varepsilon 2} - C_{\varepsilon 1})}. \tag{9}$$

Therefore if altering C_μ, then σ_ε must too be altered.

The Standard k–ε Model does not just under-predict TKE levels for boundary layer flows but also has a tendency to under-predict TKE within street canyon flows. Solazzo [15] found that reducing the values for parameters σ_k and σ_ε from the default values resulted in an improved prediction of TKE within the street canyon due to an increased spread of TKE in the shear layer above the street canyon.

It is clear from previous research that alteration of the k–ε constants in some instances can lead to an improvement in predictions of TKE within street canyon and urban boundary layer flows. There is a need to better understand the uncertainties relating to these constants and find a way of reducing the range of possible values they could take. This provides the motivation for this paper, which will perform a Bayesian calibration of four out of the five Standard k–ε constants for the case of street canyon flow. Due to the interconnected nature of the boundary conditions, turbulence model and the constants it is important to note that by calibrating the constants we are examining the uncertainties connected to *both the turbulence model and the boundary conditions* at the inlet.

2. Wind tunnel set up

The data used to calibrate the CFD model were Turbulent Kinetic Energy values taken from a wind tunnel experiment carried out by Kastner-Klein et al. [2] in the wind tunnel at the University of Karlsruhe. The buildings on either side of the street were represented by two rectangular blocks. The wind direction was perpendicular to the street axis. The model of an atmospheric boundary layer was obtained through the use of small blocks placed on the wind tunnel floor. Measurements were taken using a laser velocimetry system. Velocity measurements were taken on a vertical cross section of the street at the centre of the street canyon. Fig. 1 shows a cross section of the street canyon and the measurement locations within the street.

3. CFD simulation

A fully 3-dimensional CFD simulation of the Kastner-Klein wind tunnel experiment [2] was carried out using ANSYS CFX. The dimensions of this model are given in Fig. 2. An unstructured hexahedral mesh was used for this study. A mesh refinement zone was created in between and around the buildings allowing for the capture of the details in this region. In order to ensure only a small discretization error within the CFD model, a mesh sensitivity test was carried out for the street domain. The mesh inside the street canyon was systematically varied until a mesh independent solution was reached. We tested recommendations in best practice guidelines for urban CFD simulations, that a mesh size of at least $H/10$ (where H is the height of the building) should be used if the correct flow features are to be captured surrounding the building [16]. Therefore the maximum cell size close to the ground and within the area of interest was taken to be 0.012 m. Five mesh sizes were tested. The different mesh sizes are described in Table 2. The minimum mesh size is the mesh size within the area of interest, which is here the centre portion of the street canyon. The mesh outside this region is increased with an expansion ratio of 1.2 to a maximum size of 0.03 m. Velocity, TKE and dissipation profiles were taken from within the centre of the street canyon for all five meshes and are compared in Figs. 3–5. The results show a significant sensitivity of TKE to mesh size. At the roof top level reducing the mesh size from 0.012 m ($H/10$) to 0.003 m ($H/30$) results in 70% increase in TKE. It appears that

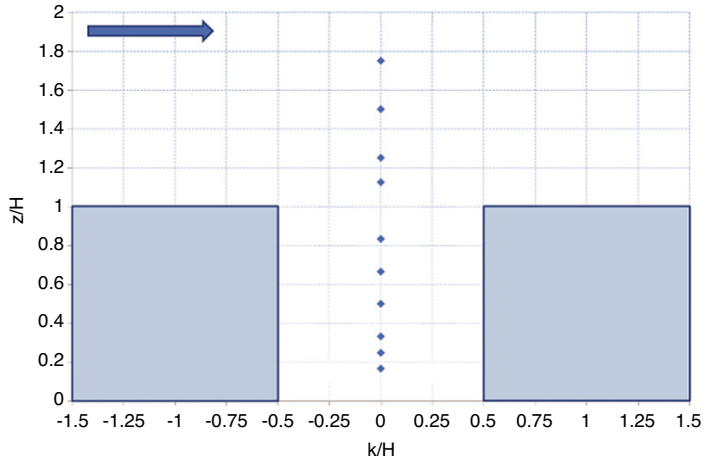

Fig. 1. Diagram showing location of measurement points within the street canyon. The two shaded blocks represent the buildings on either side of the street. The x and z axis are normalized by the height of the building H.

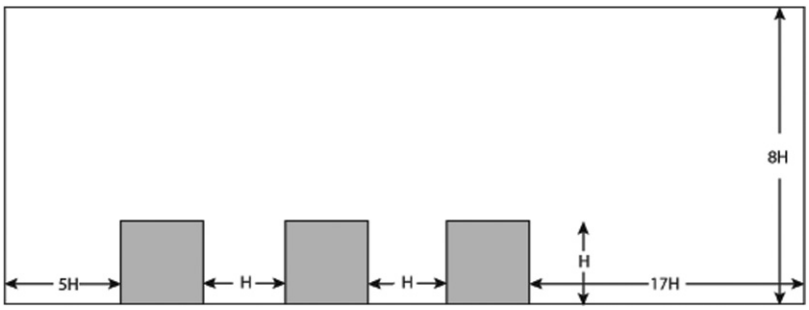

Fig. 2. Geometry of the street canyon. The TKE profiles were taken inside the canyon (Figure not to scale).

Table 2
Meshes considered in the mesh sensitivity test.

Mesh	Minimum cell size	Maximum cell size	Total number of cells
Mesh 1	0.012	0.03	690 400
Mesh 2	0.008	0.03	1338 300
Mesh 3	0.006	0.03	1578 812
Mesh 4	0.004	0.03	3099 600
Mesh 5	0.003	0.03	5142 980

the mesh within the canyon and immediately above the canyon needs to be fine enough to capture the production of TKE at the leading edge of the upwind building, without this, gross underestimation of turbulence levels may occur. The often quoted guideline of a cell size of $H/10$ within and immediately above the canyon is reasonable if only a qualitative prediction of flow patterns is needed. If accurate predictions of turbulence quantities are required, then a much finer mesh is recommended. The software code CFX places certain restrictions on the size of the mesh closest to the wall based on the size of the sand grain roughness used, therefore it would not be possible to reduce the mesh size beyond mesh size 5 without an alteration to the sand grain roughness height. There was little to no difference in velocity profiles between meshes 4 and 5 and a maximum difference of 5% was found for the TKE values. Therefore it was decided that mesh 4 could provide a reasonable level of accuracy for this study for a computationally reasonable cost.

To specify the boundary conditions at the inlet, Eqs. (6)–(8) following Richards and Hoxey [14] were chosen, due to the fact they are consistent with the k–ε model and easy to adapt to other situations. The outlet boundary was set to

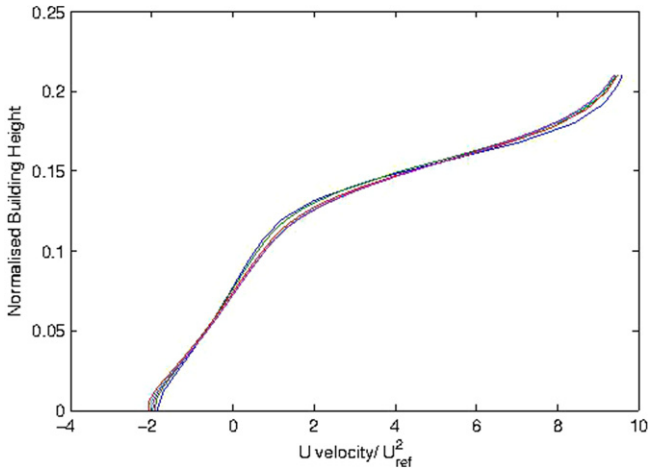

Fig. 3. Vertical profiles of streamwise velocity component u. Mesh 1—blue, mesh 2—green, mesh 3—red, mesh 4—light blue, mesh 5—purple. (For interpretation of the references to colour in this figure legend, the reader is referred to the web version of this article.)

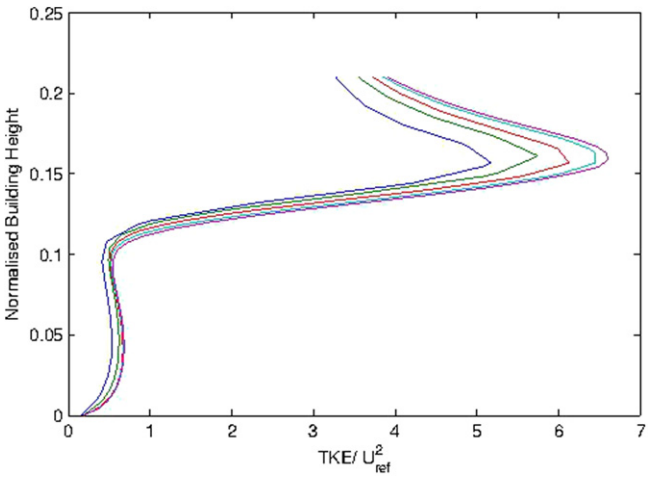

Fig. 4. Vertical profiles of TKE. Mesh 1—blue, mesh 2—green, mesh 3—red, mesh 4—light blue, mesh 5—purple. (For interpretation of the references to colour in this figure legend, the reader is referred to the web version of this article.)

outflow with static pressure 0 Pa. The top of the domain boundary was set to a wall boundary with a specified shear stress of $\tau = 0.36$ Pa, based on the wind tunnel data measurements, which determined a value of 0.55 m/s for the frictional velocity u_*.

In order to maintain a homogeneous atmospheric boundary layer flow, a sand grain roughness was applied to the wall boundaries in CFX. This had to match the roughness blocks that had been placed on the floor of the experimental wind tunnel. The recommended sand grain roughness in the literature [9] for other cases is 30 times the roughness length which would give a value of 0.024 m for this experiment. However, CFX specifies that a cell height of twice the size of the sand grain roughness must be used at the wall boundary; this would have resulted in a coarse mesh close to the wall, thus on the basis of the mesh sensitivity analysis of the empty domain, a sand grain roughness of 0.006 m was chosen.

It was then necessary to use a wall function to model the flow in the region closest to the wall. Within this region the law of the wall was applied:

$$u^+ = \frac{1}{k}\ln(y^+) + C \tag{10}$$

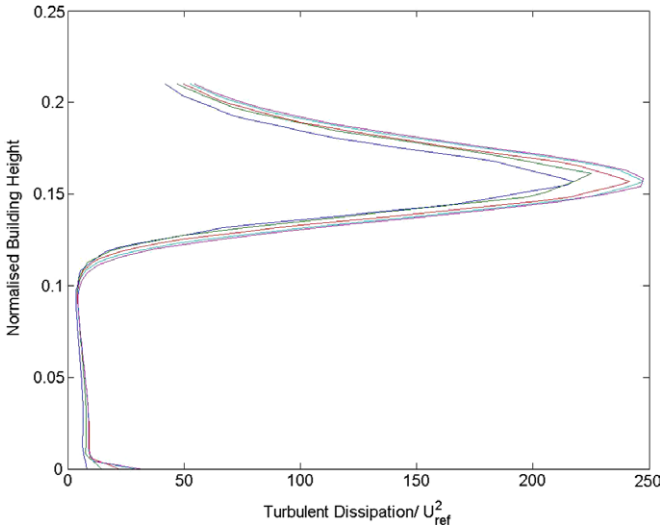

Fig. 5. Vertical profiles of turbulent dissipation. Mesh 1—blue, mesh 2—green, mesh 3—red, mesh 4—light blue, mesh 5—purple. (For interpretation of the references to colour in this figure legend, the reader is referred to the web version of this article.)

where u^+ and y^+ are dimensionless variables given by:

$$u^+ = \frac{U_t}{u_*} \tag{11}$$

$$y^+ = \frac{u_* \Delta y}{v} \tag{12}$$

with U_t the known tangential velocity at a distance Δy from the wall, u_* the frictional velocity in the wall region and v the kinematic viscosity. This formula was applied to the region containing the street geometry. Outside this region the formula must be adapted to account for roughness, which causes turbulence in the shear layer and shifts the logarithmic profile downwards. Thus, the law of the wall is modified in the following way:

$$u^+ = \frac{1}{k} \ln(y^+) + B - \Delta B \tag{13}$$

where $B = 5.2$. The downward shift ΔB can be expressed as:

$$\Delta B = \frac{1}{k} \ln(1 + 0.3 h_s^+) \tag{14}$$

where h_s^+ is defined as

$$h_s^+ = h \frac{u_\tau}{v}. \tag{15}$$

4. Statistical calibration

The calibration process consists of putting distributional assumptions (prior distributions or simply priors) on the calibration (also called tuning) parameters $C_{\varepsilon 1}$, $C_{\varepsilon 2}$, σ_k and C_μ before comparing with observations, and letting the information contained in the data update this a priori assumption to get as a result a posterior distribution of the calibration parameters. The advantage of such a Bayesian analysis [1] over standard estimation of parameters (e.g. by minimizing the differences between observations and simulator outputs) lies mainly in the ability to retrieve a full description of the uncertainties about the parameters and consequently about the simulator outputs. Moreover, the possibility for the modellers to express their – uncertain – scientific beliefs in terms of priors on the parameters enables a natural integration of scientific knowledge and evidence given by measurements.

It was decided to calibrate four out of the five k–ε model constants and not σ_ε due to its strong interdependence on the other model constants. Formula (9) was used to set the value of σ_ε. For simplicity we now denote $C_{\varepsilon 1}$ and $C_{\varepsilon 2}$ as

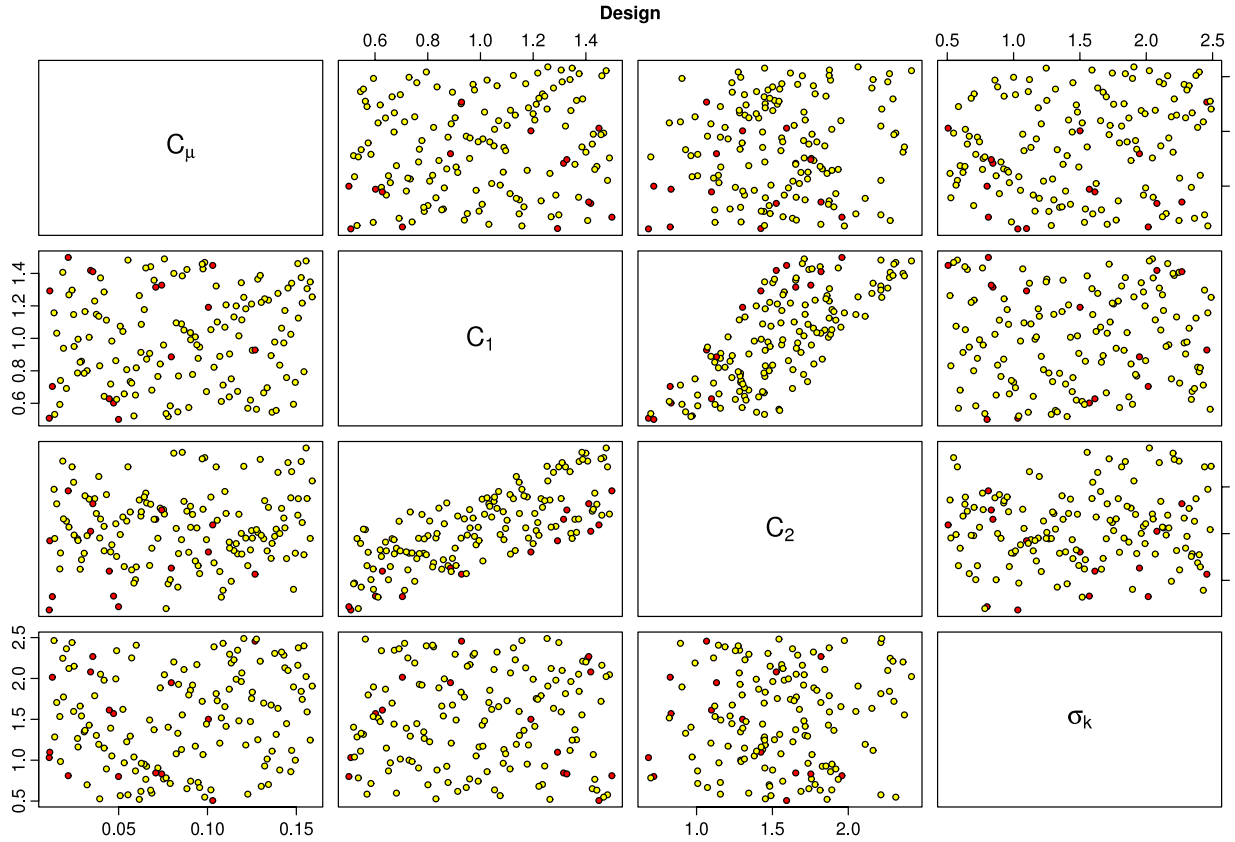

Fig. 6. Design of calibration parameters. Values highlighted in red did not achieve convergence in the CFD model. (For interpretation of the references to colour in this figure legend, the reader is referred to the web version of this article.)

C_1 and C_2. The intervals explored for the calibration constants were chosen based on typical values suggested for the model constants and how these had been changed in the past, see Table 1. We put uniform priors on these parameters, allowing for equal initial probability of being at any location in these intervals.

The convergence criteria for the CFD simulations was set to 1×10^{-4} with an imbalance of less than 0.1% as well as velocity and turbulence being monitored at several points to ensure stable conditions were reached. We performed a total of 150 CFD runs. Of these 150 runs 135 converged successfully. Fig. 6 illustrates which of the calibration parameters did not achieve convergence. It appears that these failures occur when C_1 is relatively close to C_2 and thus leads to numerical stability issues in (9) as σ_ε becomes too close to zero. $C_2 > C_1$, which is not allowed by our choice of prior, would make σ_ε negative and provoke an even more serious numerical problem. One could have optimized better the design for these CFD runs, described in the following section, by not allowing close values of C_2 and C_1 and thus saved some computational runtime.

The complete set of inputs $x = (h, \theta)$ consists of parameters divided into two categories: the known parameters (normalized height h in $[0, 2]$) and the unknown calibration parameters $\theta = \left(C_1, C_2, C_\mu, \sigma_k\right)$. We denote by $y^M(x)$ the empirical output of the computer model as a function of $x = (h, \theta)$ and $\eta(x)$ the expected output of the computer model as a function of $x = (h, \theta)$. The difference between $y^M(x)$ and $\eta(x)$ is the numerical intrinsic error. The computer code output $\eta(x)$ is an approximation of the reality $y^R(h)$. The notation used emphasizes that physical observations are only made at values of the observable parameter, h. To learn about the values of the calibration parameters, the CFD model is run at inputs x in a design (i.e. choice of values) D^M. Field data (i.e. TKE observations taken from the wind tunnel) $y^F(h)$ are collected at a number of inputs heights h.

The design D^F (the locations at which observations are collected) are given by Kastner-Klein et al. [2]. For our design of experiments D^M corresponding to the calibration parameters, we use a maximin Latin Hypercube (LHS) design [17], whose 1-D and 2-D projections are seen in Fig. 6. With this design we try to cover as much space as

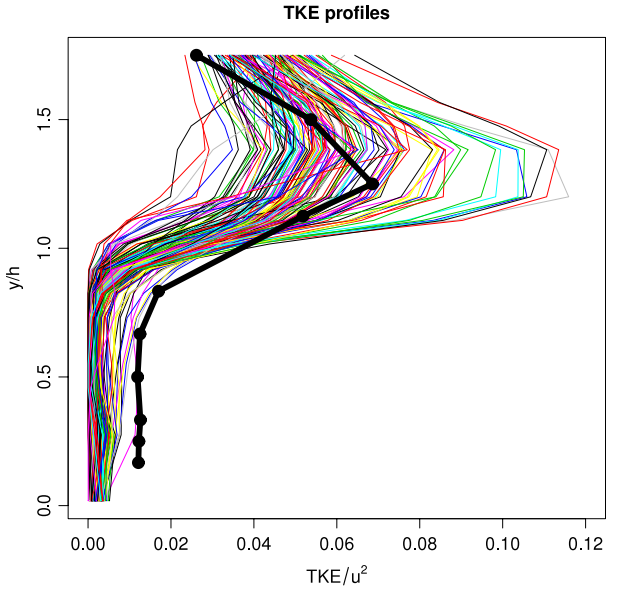

Fig. 7. Normalized TKE data from wind tunnel (circles) and CFD simulation (coloured lines) against height normalized by the height h of the buildings. The profile was taken at the centre of the street canyon. (For interpretation of the references to colour in this figure legend, the reader is referred to the web version of this article.)

possible in the four-dimensional space of the calibration parameters with $n = 135$ runs (after excluding the runs that did not converge). For the spatial coordinates of the computer design D^M, we choose the same locations as the experimental design. Fig. 7 shows the CFD computed TKE values at these heights. This is the first step in our study.

The following equations constitute an extension of Kennedy and O'Hagan [1] as they specify the intrinsic CFD model numerical error. They describe the relationships between the CFD model and the observations at the design points, using bias $\delta(h)$, intrinsic CFD model numerical error ν_η and observation error ν (both assumed constant across heights h):

$$y^M(h,\theta) = \eta(h,\theta) + \nu_\eta \tag{16}$$

$$y^R(h) = \eta(h,\theta^*) + \delta(h) \tag{17}$$

$$y^F(h) = y^R(h) + \nu. \tag{18}$$

Here, θ^* is used to represent the true (unknown) values of the calibration parameters. These equations suggest that even if the CFD model were run at the true values of the calibration parameters, it would still be a biased representation of reality. Thus the model can never perfectly match observations without some additional process of adjusting for model errors. It is crucial that such a discrepancy (or bias) term be introduced in order to avoid overfitting the data with an unrealistic choice of parameters. Furthermore, the bias must vary according to height, as the CFD model shortcomings are strongly dependent on height. This is unnecessary for the observation error and the numerical error in the CFD model as these may vary only very slightly according to height and are much smaller than the model bias.

Because the simulator output $\eta(\cdot)$ is unknown except at the design points D^M, we assume that the unknown function follows a Gaussian stochastic process (GP) distribution. That is, we model the simulator responses $\eta(x), x \in R^p$ (here $p = 5$ since D^M is over a range of C_1, C_2, C_μ, σ_k and h, values), as coming from a multivariate normal distribution with mean μ and $N \times N$ variance–covariance function Σ conditional on the observed outputs from the N runs. Since we initially standardize the entire set of responses (CFD model and observed) by the mean and standard deviation of the CFD responses, $\mu = 0$ above and the variability in the simulator $(1/\lambda_\eta)$ below is approximately 1. Thus, we approximate the CFD model by specifying a distribution of functions that interpolate the response $\eta(x)$ in between the design points x in D^M. The random function is certain at the design points, and uncertain at untried points.

To specify Σ according to the calibration parameters we use a product Gaussian variance–covariance. Thus, the (i, j)th element of Σ, $\mathrm{cov}(\eta(x_i), \eta(x_j))$, is (conveniently using the notation θ_4 for h):

$$\frac{1}{\lambda_\eta}\exp\left(-\sum_{k=1}^{4}\beta_k|\theta_{ik}-\theta_{jk}|^2\right).$$

The notation θ_{ik} denotes the ith design point in D^M for θ_k. The hyperparameters λ_η (the precision of the GP model), β_k (which we call "correlation hyperparameters") are to be estimated from the model output and the observations as described below. The unknown bias function $\delta(h)$ is also modelled as a GP random function with mean 0 and correlation matrix with precision λ_δ and correlation parameter β_5. Finally, the random error and intrinsic error components are modelled as independent $\nu \sim N(0, 1/\lambda_\nu)$ and $\nu_\eta \sim N(0, 1/\lambda_{\nu_\eta})$. Only the θ's are deemed to be calibration parameters, or quantities to be tuned for the CFD model to perform better. All the other quantities, such as observation and numerical errors, as well as the hyperparameters, are only auxiliary quantities for the analysis (but are of interest nevertheless).

The likelihood can be written, for a joint vector of given observations y^F and CFD model outputs y^M,

$$\begin{bmatrix} y^F \\ y^M \end{bmatrix} \sim MVN(0, \Sigma_y) \tag{19}$$

where

$$\Sigma_y = \Sigma_\eta + \begin{bmatrix} \Sigma_b & 0 \\ 0 & 0 \end{bmatrix} + \begin{bmatrix} \Sigma_\nu & 0 \\ 0 & \Sigma_{\nu_\eta}. \end{bmatrix}. \tag{20}$$

For the estimation of the calibration parameters, and all the other quantities, we employ the Markov Chain Monte Carlo (MCMC) algorithm, see e.g. Chib and Greenberg [18]. The code we are using is publicly available as supplementary material from Han et al. [19]. The chains are dependent random samples that ought to be distributed in the long run as the so-called posterior distributions of the parameters of interest, which are combinations of prior information about the values of these parameters and the information about the parameters provided by the measurements. We then retrieve the posterior distributions of the various calibration parameters, which allow us to make inferences and quantify our uncertainty about the true values of these unknown quantities.

All the unknowns in the model (i.e. the calibration parameters and the hyperparameters such as variances – here actually precisions – and correlation parameters β's) require specified prior distributions which represent uncertainty about the values of these parameters before any data is collected. The following choices are made for the priors:

- To represent vague prior information about the true calibration parameter values, we specify a uniform prior distribution over the interval on which they were sampled for simulator runs.
- To model the correlation hyperparameters in Σ, we conservatively place most of its prior mass on values for the corresponding correlations near 1 (indicating an insignificant effect). Similarly, conservative priors were used for the hyperparameters associated with the correlations in the bias function.
- Gamma prior distributions were used for each of the precision (i.e. inverse of the variance) hyperparameters λ_η, λ_δ and λ_ν. Specifically, we use priors $\lambda_\eta \sim \mathrm{GAM}(10, 10)$ (with expectation 1 due to standardization of the responses), $\lambda_\delta \sim \mathrm{GAM}(10, .3)$ (with expectation around 3% of standard deviation of the standardized responses), and $\lambda_\nu \sim \mathrm{GAM}(10, .03)$ 0.3% and $\lambda_{\nu_\eta} \sim \mathrm{GAM}(10, .001)$ 0.01%. These prior assumptions are based on our original scientific understanding of the problem: we want the CFD model to capture most of the variations in order to tune our calibration parameters, and the bias ought to be small as a result. Observation errors must be an order of magnitude smaller, and numerical errors are usually more than an order of magnitude smaller than observation errors. Obviously data, through our Bayesian analysis, can sway these priors, as it does for the bias that is much larger than 3% of the TKE variations in the CFD in the lower part of the street canyon (see Fig. 10 in the next section).

The choice of relatively strong priors for the variances above enables us to distinguish between the bias and the observation errors. Indeed, this is done to overcome the confounding issue as these variations are additive. The prior information about observation and numerical errors assumes that these variations represent a realistic choice, but more informed priors could be derived from the experiments directly or by analysing further the CFD model. However,

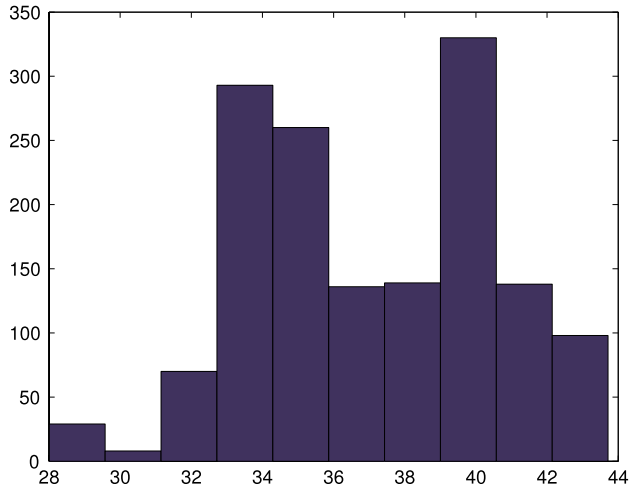

Fig. 8. Posterior distribution for observation error.

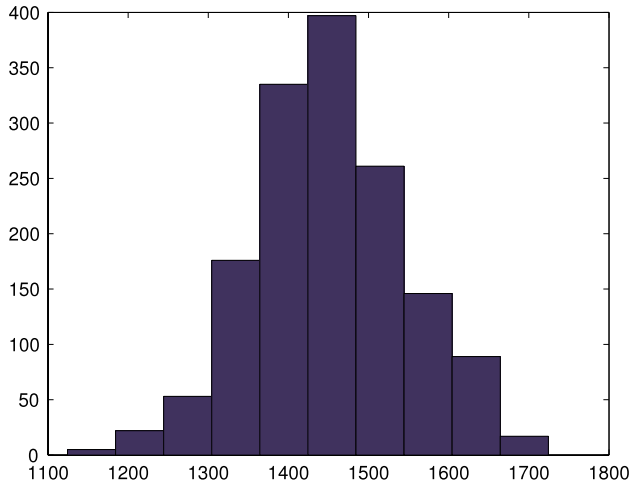

Fig. 9. Posterior distribution for numerical error.

the benefit of this large effort is likely to be tiny in our opinion, if any, as data will sway this prior through the Bayesian approach. Because our choice of priors makes the full conditional distributions of the unknowns difficult to sample, we implement a Metropolis–Hastings algorithm to explore the multidimensional space of parameters. The algorithm makes use of a proposal distribution to draw a future value conditional on the current state. Then this move is either accepted or rejected according to a random toss with a probability of acceptance that depends upon the target distribution. This eventually yields draws from the target distribution (here the posterior). We used multiple chains to confirm the convergence towards a stationary posterior distribution (after an initial burn-in period), saving wall-clock time by running the chains in parallel.

5. Results

5.1. Impact on TKE

The results of all 135 CFD runs are shown in Fig. 7. The normalized TKE values are plotted against the normalized height. We can see the wide spread in TKE results produced by varying the k–ε model constants. This figure describes the sensitivity of the model to the values used for the calibration parameters. It highlights the importance of choosing the most appropriate values for these constants and the need for calibration.

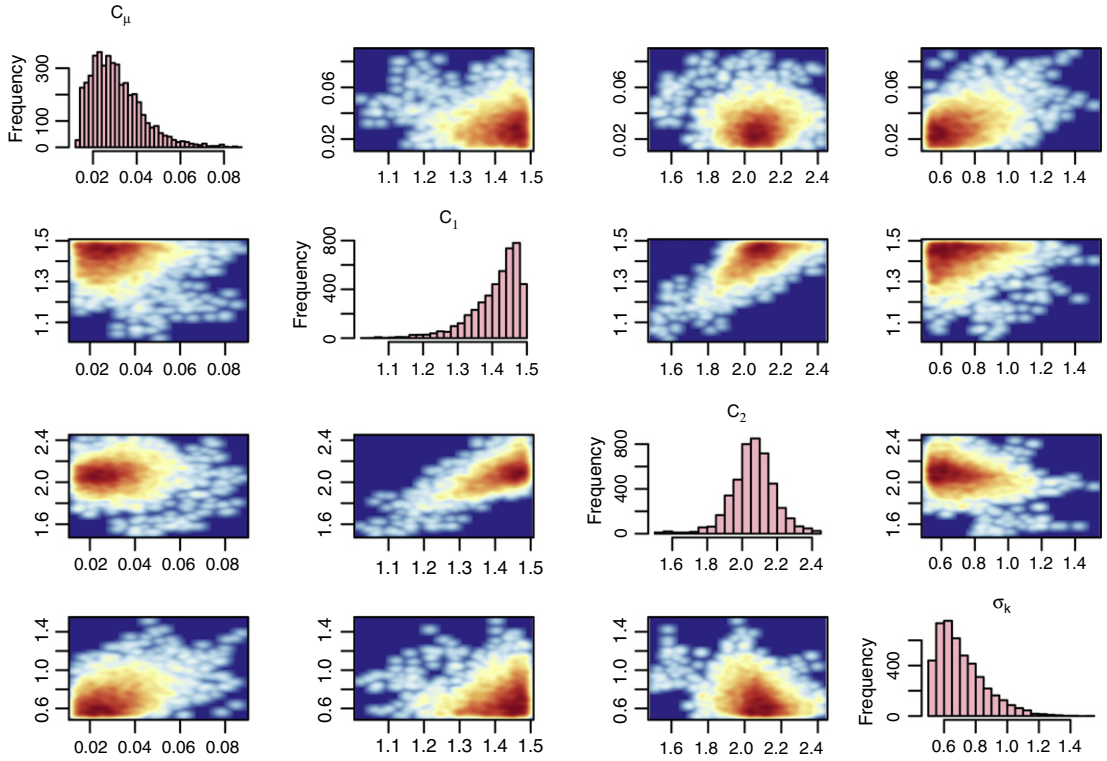

Fig. 10. Joint posterior distributions for the calibration parameters.

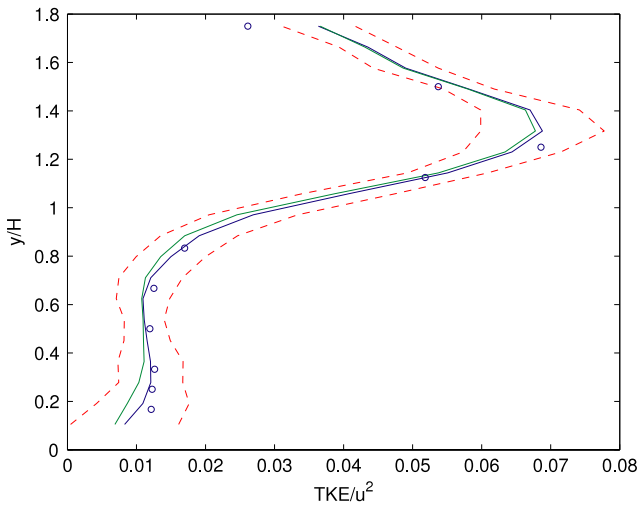

Fig. 11. Figures showing observations (circles), the predictions given by the emulation of the CFD model (green) and predictions with the addition of the estimated bias (blue). The red dashed lines are the 95% confidence interval bands. (For interpretation of the references to colour in this figure legend, the reader is referred to the web version of this article.)

The posterior for the numerical errors and observation errors, are respectively small. Figs. 8 and 9 respectively show the hyperparameters λ_v and λ_{v_η}. Their inverses are respectively smaller than $1/28$ and $1/1100$ compared to TKE's variations (normalized to 1). Hence, they are unlikely to have a big impact on the calibration results.

Fig. 10 displays the histograms for the posterior draws for all four calibration parameters. From the distribution of the histograms we can infer information about the preferred values for each parameter and uncertainty related to that

parameter. The posterior for C_μ shows values at the lower end of the interval are given higher probability of providing a better match with the experimental data. In particular we can see that the default value of 0.09 is not deemed a suitable value in this context, as there is low probability that this would be the best fit. As noted earlier, using the boundary conditions suggested by Richards and Hoxey [14] the TKE value at the inlet tends to be under-predicted when using the default value of C_μ. To avoid this under-prediction, researchers in the past have decreased the values of C_μ thereby increasing the TKE value (see Eq. (7)). This is reflected by the posterior distribution. The posterior for parameter σ_k is highly skewed towards the lower values of the interval which suggests the chosen interval of 0.5–2.5 was not wide enough. The posterior shows values closer to 0.5 are more favourable. This is consistent with findings of Solazzo [15], who changed the values for parameters σ_k and σ_ε for a similar street canyon configuration and found that decreasing the value of σ_k from the default value of 1 to a value of 0.53 had the effect of spreading the width of the TKE profile in the shear layer. This lead to a greater proportion of the TKE being advected down into the street canyon, reducing the under-estimation of TKE within this area. The preferred values we find for C_1 and C_2 are similar to the default values suggested by Launder and Spalding [12].

By plotting the joint posterior distributions we can see how the probability distributions of the parameters are connected (see Fig. 10). From these figures we can see how much the space of plausible model constants is reduced through the process of the calibration. In order to utilize this result a suggestion would be to take a sample from this posterior distribution of parameter combinations and run the CFD models again with these new calibration values. Thus rather than giving a single TKE output at each location we would have a range of TKE values that would better represent the uncertainty present within the CFD model and by sampling from the posterior we are able to narrow down the uncertainty of our output.

The final stage in the calibration process is to produce an emulator of the CFD model. This extracts all the information contained within the CFD runs regarding the calibration parameters and their uncertainties and uses it to produce predictions of the TKE values at specified heights. The mean posterior bias can be seen in Fig. 8, as the difference between the mean posterior for the CFD model, i.e. the emulator, and the mean posterior for the predictions, i.e. emulator + bias. As expected typically the bias is slightly larger within the street canyon (normalized heights less than 1) due to the CFD model's tendency to under-predict the TKE in this area as is illustrated by Fig. 4. This would suggest that accurate prediction of the TKE values within the street canyon cannot be obtained purely by tuning of the k–ε model constants.

The bands about the predictions (shown by the red dashed line in Fig. 11) reflect all sources of uncertainties: in the unknown calibration parameters, in the computer model GP parameters (variance and correlation length), in the bias' GP parameters (variance and correlation length), and in the errors (numerical and observation). The bands are wider where more uncertainty can arise, especially at the upper and lower boundaries of the canyon, where no information is available on the other side to constrain the uncertainties further. We expect to observe more or less 95% of the observations to lie in these uncertainty bands based on this calibration: a formal way to verify this would be to carry out a leave-one-out diagnostic where we would repeatedly remove one observation from the analysis and confirm that, 95% of the time, the new prediction would include this value. This has been done for this calibration code in other modelling situations for a thermosphere–ionosphere electrodynamics general circulation model [20] and for tsunami simulations [21]. Overall, the plot in Fig. 11 (except for the boundary issue) seems to reflect that the confidence bands across height are reasonable. Hence, we chose to not do a leave-one-out analysis here.

5.2. Joint calibration with the von Karman constant

The value of the von Karman constant κ may not be considered known or universal, see McKeon et al. [22], Oliver and Moser [23], and Edeling et al. [9]. Hence, we carried out another calibration using the exact same conditions as in the previous calibration with four parameters, but with the addition of a fifth parameter κ. A uniform distribution over the interval $[0.38, 0.45]$ was chosen as prior distribution for κ. We collected $n = 150$ runs of the CFD model based on a maximin Latin Hypercube (LHS) design.

Fig. 14 shows the failed convergence of the sample paths for κ and for σ_k (the one parameter which converges and changed value in the main successful calibration). Each includes 3 independent Markov chains for this investigation, and required around 3 days of CPU time on a 4 core machine as the complexity of the calculations increases dramatically with the size of the problem. The calibration fails to calibrate κ as well as the other parameters. Indeed, by adding the extra parameter κ, the calibration becomes a much more difficult exercise. This is due to the fact

that there is too little information in the observations to tune κ. Overall the failure of the calibration of the set of parameters can be explained in two ways. Either κ adds another level of uncertainty to the analysis or the added computational complexity does not allow the calibration to succeed (but might with more observations and model runs). Our prior interval [0.38, 0.45] is already narrow compared to Edeling et al. [9] who let κ vary within [0.30, 0.60] and obtained wide ranges of calibrated κ values fully covering the [0.30, 0.50] range. One could potentially resolve the convergence problem by constructing a more informative prior (e.g. a narrower range or a sharper distribution for κ within [0.38, 0.45]). But then, the range would be too small to allow enough sensitivity in model outputs in order to make use of the information contained in the observations; the prior would overwhelm the signal from the data. Both our attempt and the ones from Edeling et al. [9] seemingly point to a need for much more precise and helpful observations, combined with more runs for many values of κ to confidently infer appropriate values of κ.

6. Discussion

The results presented here are found to apply very specifically to the case study under examination, and cannot readily be applied to other fluid flow models, or even to other models of street canyon flows. We calibrate the constants for the specific case being examined. The nature of the general k–ε model constants first found by Launder and Spalding [12] is that they were determined on the basis of being the best fit for a wide range of fluid flows. This makes them a suitable first step in setting up a k–ε model, but when higher accuracy is desired they are found to be inadequate for many case studies and have to be modified; there is often no argument put forward for the modification and they are simply chosen on the basis of providing the best fit to a data set. By performing a bespoke, sophisticated calibration for a street canyon model we obtain parameters that are the best possible fit for this case. Inevitably, this will make them less transferable to other types of flows.

This is seen quite convincingly in examining the flow velocities. For the case presented above, the TKE calibration resulted in improved representation of TKE profiles within the street canyon, but the impact on flow velocities was minimal and in fact the modelled vortex flow within the street both before and after calibration was just as expected from experimental results. However, in our previous research [24], a fast, 2.5 dimensional simulation was performed using ANSYS CFX. Logarithmic profiles were specified for the inlet boundary conditions on the basis of providing a best fit to experimental data, following Kastner-Klein et al. [2], Di-Sabatino et al. [25]. The CFD model was then run and calibrated for only 3 parameters: C_1, C_2, C_μ. Based on the posterior histograms, values of $C_1 = 1$, $C_2 = 2.1$, $C_\mu = 0.12$ were selected as providing the most improved model performance. Thus, using the relationships mentioned above, the values of $\sigma_\varepsilon = 0.42$ and $\sigma_k = 0.462$ were found (some of these values are significantly different from those from our model presented above). The CFD model was run again with the new choice of calibration parameters. The results for the modified CFD model, as shown in Glover et al. [24], are presented here again for comparison with the model presented here. Qualitative comparison of the CFD flow patterns against the wind tunnel observations shows the improvement produced by the modification of the parameters. The size of the flow separation and vortex produced above the upstream building in that study was reduced (Fig. 12), and the centre of vortex contained within the street canyon moved down towards the centre of the street. A quantitative comparison is shown in Fig. 13 which shows the TKE profiles taken from the centre of the street canyon, demonstrating improved TKE predictions after modifying the CFD model. These results are in line with results from other research (e.g. Dunn et al. [6]) that found that model coefficients had a significant effect on stream wise mean velocity, turbulence intensity, and the location of the reattachment point.

As discussed in Section 1.4, a lack of consistency between the inlet boundary conditions, the turbulence model chosen and its constants, creates problems of decay in the turbulence profiles downstream and makes it difficult to generate the correct Atmospheric boundary layer flow at the area of interest in the numerical domain. In Glover et al. [24] these modelling problems were in effect overcome by the calibration, which caused a greater improvement to the results of the model than the calibration presented here, because the model was not as tightly specified.

Thus, it becomes clear that we create here a bespoke calibration, producing case specific constants. The results can be transferred to other similar case studies on the basis that we provide an estimate of upper and lower bounds for the values that these constants could reasonably be assumed to take for models of similar flows. It would be of interest to attempt a series of case studies with slightly varying geometry and test how different the calibrated constants would be for the various cases. This is beyond the scope of the present paper, due to the high computational efforts required in simulation of a full Atmospheric boundary layer flow, and is recommended for future research.

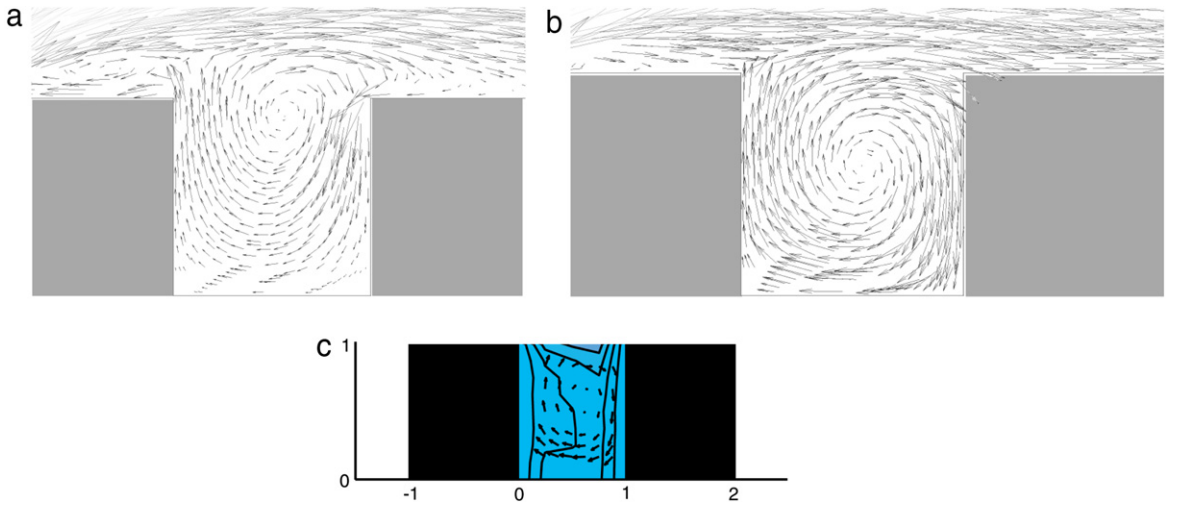

Fig. 12. Vector plot showing velocities for (a) un-modified CFD model, (b) CFD model with modified constants [24], (c) results from wind tunnel experiment, following Kastner-Klein et al. [2].

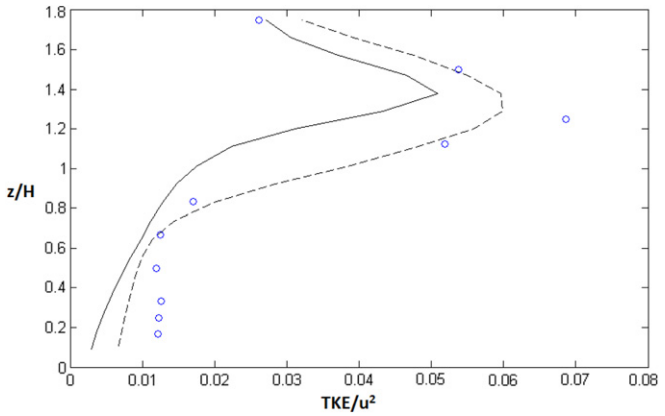

Fig. 13. Normalized TKE profiles from CFD model with un-modified constants (black line), modified constants (dashed line) and wind tunnel data (circles), following Glover et al. [24].

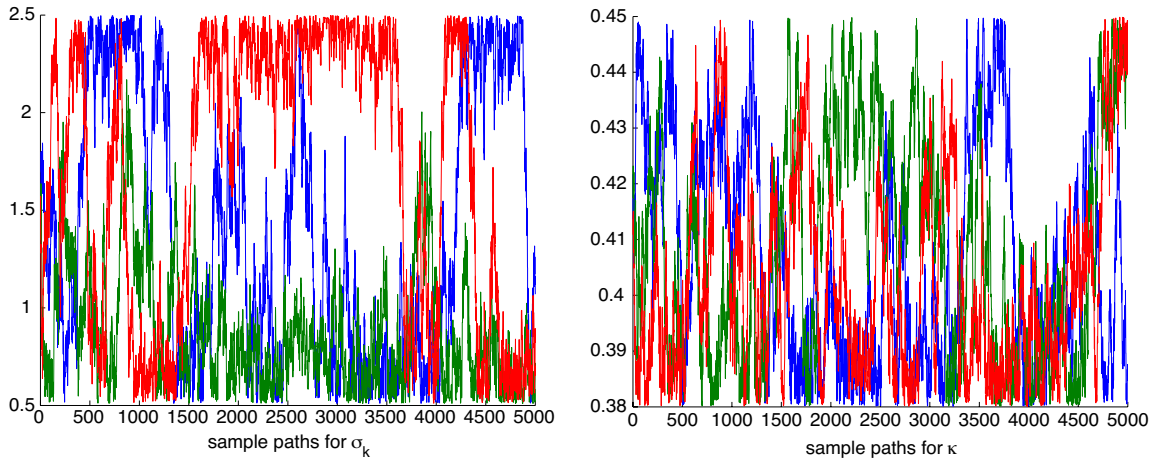

Fig. 14. Three sample paths for the posterior distributions for σ_k and κ; joint calibration with the von Karman constant.

7. Conclusion

In this paper we demonstrated how Bayesian calibration can be used to assess the uncertainties relating to the constants contained within the standard k–ε model, when used to model street canyon flow. We have demonstrated that there is a bias in the k-ε model which leads to the under-prediction of TKE within the street canyon. We have shown that the default values for these constants often used in simulations do not necessarily provide the best match with experimental data. We have also seen that purely tuning these constants cannot provide a perfect match with experimental data. Posterior distributions showed lower values for C_μ and σ_k are more likely to give improved prediction of TKE when compared with experimental data.

We have also suggested some useful applications for the Bayesian calibration process for CFD simulation for various types of flows, even complicated ones with complex boundary conditions and large uncertainties. For flows with limited experimental data or various physical unknowns, by performing the calibration we are able to sample from a smaller parameter space thus reduce the uncertainty in the CFD output that arises from our lack of knowledge about the parameterization. We highlighted the ability of the calibration of TKE to improve flows even with large errors, such as when boundary conditions are not entirely consistent for the required flow, so that the use of calibration for the observations of one variable can trickle down to other variables. We finally showed with the additional calibration of κ that one needs to be careful in the selection of parameters to be tuned. Only the parameters that are likely to influence outputs should be used, and an iterative procedure might be used to screen the most important ones. Moreover, the emulation enables this sampling procedure to be employed in order to efficiently and accurately quantify the uncertainties in the CFD output.

Our procedure does not address the issue of how parameterizations can vary for different flow types. However, Edeling et al. [9] carried out separate calibrations for a set of 13 boundary-layer flows. They summarized this information across calibrations by computing Highest Posterior-Density (HPD) intervals, and subsequently represent the total solution uncertainty with a probability-box (p-box). This p-box represents both parameter variability across flows, and epistemic uncertainty within each calibration. A prediction of a new boundary-layer flow is made with uncertainty bars generated from this uncertainty information, and the resulting error estimate is shown to be consistent with measurement data. This approach is helpful, but it might be extended further by modelling proximity across flows through a distance that would relate to the flow characteristics in order to borrow strength across calibrations instead of splitting the calibrations and then merging the outcomes afterwards. This is a challenging but attractive venue for future research.

Here we have laid out the first step in our calibration process, but there are still many important questions that need to be answered. For example the Bayesian calibration could be used on several slightly different turbulence models for a particular flow, to give quantitative estimates of uncertainty to aid in the selection of the best model for the case. Unfortunately due to restraints on computer resources we were only able to calibrate a single 1-D profile with a single QoI but, with ever increasing computing capabilities and statistical approximations, calibrations which use experimental data taken from two and even three-dimensional space and calibrate against multiple QoI's are not far out of reach. However the calibration process is likely to be most useful for applications where experimental data is sparse. The question of whether we are able to apply the calibration results to other locations within our model, other quantities of interest which we did not calibrate against (and even different flow scenarios as well) is still open ended. This question is an important topic for future research for the use of calibration in CFD applications.

Acknowledgment

We would like to acknowledge EPSRC for funding this research as part of the Bridging the Gaps program.

References

[1] M.C. Kennedy, A. O'Hagan, Bayesian calibration of computer models, J. R. Stat. Soc. Ser. B Stat. Methodol. 63 (2001) 425–464.
[2] P. Kastner-Klein, E. Fedorovich, M.W. Rotach, A wind tunnel study of organised and turbulent air motions in urban street canyons, J. Wind Eng. Ind. Aerodyn. 89 (2001) 849–861.
[3] C.J. Roy, W.L. Oberkampf, A comprehensive framework for verification, validation, and uncertainty quantification in scientific computing, Comput. Methods Appl. Mech. Engrg. 200 (2011) 2131–2144.
[4] H.N. Najm, Uncertainty quantification and polynomial chaos techniques in computational fluid dynamics, Annu. Rev. Fluid Mech. 41 (2009) 35–52.

[5] O.P. Le Maitre, O.M. Knio, H.N. Najm, R.G. Ghanem, A stochastic projection method for fluid flow: I. basic formulation, J. Comput. Phys. 173 (2001) 481–511.
[6] M.C. Dunn, B. Shotorban, A. Frendi, Uncertainty quantification of turbulence model coefficients via latin hypercube sampling method, J. Fluids Eng. 133 (2011).
[7] T.A. Oliver, R.D. Moser, Bayesian uncertainty quantification applied to RANS turbulence models, J. Phys. Conf. Ser. 318 (2011) 042032.
[8] S.H. Cheung, T.A. Oliver, E.E. Prudencio, S. Prudhomme, R.D. Moser, Bayesian uncertainty analysis with applications to turbulence modeling, Reliab. Eng. Syst. Saf. 96 (2011) 1137–1149.
[9] W. Edeling, P. Cinnella, R. Dwight, H. Bijl, Bayesian estimates of parameter variability in the k–ε turbulence model, J. Comput. Phys. 258 (2014) 73–94.
[10] B. Blocken, T. Stathopoulos, J. Carmeliet, J.L.M. Hensen, Application of computational fluid dynamics in building performance simulation for the outdoor environment: an overview, J. Building Perform. Simul. 4 (2011) 157–184.
[11] W. Jones, B. Launder, The prediction of laminarization with a two-equation model of turbulence, Int. J. Heat Mass Transfer 15 (1972) 301–314.
[12] B.E. Launder, D.B. Spalding, The numerical computation of turbulent flows, Comput. Methods Appl. Mech. Engrg. 3 (1974) 269–289.
[13] P. Richards, S. Norris, Appropriate boundary conditions for computational wind engineering models revisited, J. Wind Eng. Ind. Aerodyn. 99 (2011) 257–266.
[14] P. Richards, R. Hoxey, Appropriate boundary conditions for computational wind engineering models using the k–ε turbulence model, J. Wind Eng. Ind. Aerodyn. 46–47 (1993) 145–153.
[15] E. Solazzo, Modelling dispersion of traffic-related pollutants in urban canyons and intersections (Ph.D. thesis), University of Birmingham, 2008.
[16] J. Franke, A. Hellsten, K.H. Schlunzen, B. Carissimo, The COST 732 best practice guideline for CFD simulation of flows in the urban environment: a summary, Int. J. Environ. Pollut. 44 (2011) 419–427.
[17] M.D. Mckay, R.J. Beckman, W.J. Conover, A comparison of three methods for selecting values of input variables in the analysis of output from a computer code, Technometrics 42 (2000) 55–61.
[18] S. Chib, E. Greenberg, Understanding the Metropolis–Hastings algorithm, The American Statistician 49 (1995) 327–335.
[19] G. Han, T.J. Santner, J.J. Rawlinson, Simultaneous determination of tuning and calibration parameters for computer experiments, Technometrics 51 (2009) 464–474.
[20] J. Rougier, S. Guillas, A. Maute, A. Richmond, Expert knowledge and multivariate emulation: the thermosphere–ionosphere electrodynamics general circulation model (TIE-GCM), Technometrics 51 (2009) 414–424.
[21] A. Sarri, S. Guillas, F. Dias, Statistical emulation of a tsunami model for sensitivity analysis and uncertainty quantification, Natural Hazards Earth Syst. Sci. 12 (2012) 2003–2018.
[22] B.J. McKeon, J. Li, W. Jiang, J.F. Morrison, A.J. Smits, Further observations on the mean velocity distribution in fully developed pipe flow, J. Fluid Mech. 501 (2004) 135–147.
[23] T.A. Oliver, R.D. Moser, Accounting for uncertainty in the analysis of overlap layer mean velocity models, Phys. Fluids 24 (2012) 075108.
[24] N. Glover, S. Guillas, L. Malki-Epshtein, Statistical calibration of CFD modelling of street canyon flows, in: Building simulation 2011, proceedings, Sydney, 2011.
[25] S. Di-Sabatino, R. Buccolieri, B. Pulvirenti, R. Britter, Simulations of pollutant dispersion within idealised urban-type geometries with CFD and integral models, Atmos. Environ. 41 (2007) 8316–8329.